1030 nm Multilayer Oxide Aperture VCSELs with 25 GHz Modulation Bandwidth and 40 Gb/s NRZ Transmission

Yanjing Wang[a], Cunzhu Tong *[a,b], Xiaoqian Luan[b], Ning Jiang[b], Haixia Tong [b], Lijie Wang[a,b], Sicong Tian[a]

[a] State Key Laboratory of Luminescence and Application, Changchun Institute of Optics, Fine Mechanics and Physics, Chinese Academy of Sciences, Changchun 130033, China

[b] Jlight Semiconductor Technology Co., Ltd, Changchun 130033, China

ABSTRACT

We present the design, fabrication, and performance of high-speed oxide-confined 1030 nm vertical-cavity surface-emitting lasers (VCSELs) with a short optical cavity, and multiple oxide apertures. High-speed modulation was facilitated by using the shortest possible cavity of a half-wavelength length and multiple oxide apertures to enhance the confinement of optical fields and reduce capacitance. We carefully optimized the multiple quantum wells and the doping profile in order to achieve a high-speed operation. The developed VCSELs exhibit a modulation bandwidth exceeding 25.1 GHz at 25 ℃, supporting back-to-back data rate up to 40 Gb/s under binary non-return-to-zero (NRZ) modulation.

Keywords: Vertical-cavity surface-emitting laser, high-speed, multi-oxide layer, modulation bandwidth

1. INTRODUCTION

The short-reach optical interconnects used in data centers are dominated by 850 nm GaAs-based vertical-cavity surface-emitting lasers (VCSELs) and multimode fiber (MMF) links, typically reaching up to 100 meter in link length [1-3]. However, the distance is fundamentally limited by the high chromatic dispersion of fiber and attenuation at this wavelength [4, 5]. At 850 nm, the fiber chromatic dispersion is as high as~85 ps/nm/km and the attenuation exceeds 2 dB/km [6, 7]. With data centers growing in size, the increased demand for longer reach optical interconnects (up to 2 km in large scale data centers [5]) drives the development of longer wavelength VCSELs so that the reach limitations of the 850 nm multimode links can be overcome.

The ideal wavelength is 1310 nm where chromatic dispersion is near zero and the attenuation of MMF is only~0.4 dB/km [6, 7]. Up to now, 1310 nm VCSELs have been developed based on quantum-dot [8] and InP material [9, 10]. However, the GaAs-based VCSEL technology, which is superior to the InP-based in terms of speed, efficiency, manufacturability and cost-efficiency, can only be extended to~1100 nm using conventional compound semiconductors without compromising reliability [11]. This has created an interest in GaAs-based VCSELs at wavelengths just below 1100 nm where the fiber chromatic dispersion is~30 ps/nm/km and the attenuation is below 1 dB/km [6, 7]. a large improvement with respect to 850 nm.

For the purpose of extending the wavelength without compromised reliability [11, 12]. GaAs-based VCSEL with wavelength ~1100 nm was developed. Using the strained InGaAs/GaAs quantum wells (QWs) with doped barriers for high differential gain and reduced gain compression, oxide-confined VCSELs at 1090 nm with a modulation bandwidth of 20 GHz were demonstrated in 2006 [13]. Then a bottom-emitting VCSEL with a bandwidth of 18 GHz using multiple oxide apertures for low capacitance were demonstrated [14]. Furukawa demonstrated 20 GHz bandwidth oxide confined 1060 nm VCSELs using double intra-cavity structure and a dielectric top distributed Bragg reflector (DBR) [15-18]. however, it is significant different from the commercial VCSELs in structure and processing. Recently, 1060 nm VCSELs utilizing strained InGaAs/GaAsP QWs and multiple oxide apertures with a bandwidth of 22 GHz were realized with similar techniques of commercial VCSELs [19-21]. However, the bandwidth of GaAs-based VCSELs emitting at ~1060 nm is still somewhat behind 850 nm and 980nm VCSELs, which are respectively 30 GHz [22-24] and 35 GHz at room temperature [25].

*tongcz@ciomp.ac.cn

SPIE-CLP Conference on Advanced Photonics 2022, edited by Xu Liu, Anatoly Zayats, Xiaocong Yuan, Proc. of SPIE Vol. 12601, 126010A
 · 0277-786X · doi: 10.1117/12.2666696

In this letter, we present a GaAs-based 1030 nm VCSEL with strained InGaAs/GaAsP QWs, a short optical cavity, and multiple oxide apertures. The modulation bandwidth of the VCSEL is 25.1 GHz and the data transmission at rates up to 40 Gb/s is demonstrated at 25 ℃. The design and fabrication of the VCSEL are presented in Section 2 and their static characteristics are presented in Section 3. Section 4 is devoted to the small-signal modulation. Section 5 is devoted to the large-signal modulation and a conclusion is presented in Section 6.

2. VCSEL DESIGN AND FABRICATION

The 1030 nm VCSEL epitaxy material was grown by metalorganic chemical vapor deposition (MOCVD). The first 26 pairs bottom DBR are made of AlAs/GaAs to reduce the thermal impedance. All other mirrors are made of $Al_{0.9}Ga_{0.1}As$/GaAs. The DBRs are with graded interfaces and modulation doping for the low resistance and internal optical loss. Multiple oxide apertures are placed in the p-DBR just above the active region. For high longitudinal optical confinement, we use a half-wavelength (λ/2) thick cavity. The active region is positioned in a thin separate confinement heterostructure at the center of λ/2 cavity. The periodic antinode of optical standing wave is designed exactly at the position of the active region.

In the active region, we use three partially strain-compensated InGaAs/GaAsP QWs, with net compressive strain. Above the active region is a p-DBR stack with 2 pairs of $Al_{0.98}Ga_{0.02}As$/GaAs, 4 pairs of $Al_{0.96}Ga_{0.04}As$/GaAs. Transverse optical and current confinement is mainly provided by two $Al_{0.98}Ga_{0.02}As$ layers after wet oxidation. The four $Al_{0.96}Ga_{0.04}As$ layers are used to reduce the parasitic capacitance of oxide apertures.

The fabrication process starts with a 22-μm diameter DBR mesa defined by inductively coupled plasma (ICP) dry etching. A laser interferometry apparatus was used to monitor the etching. Right after the dry etching, the sample was sent to an oxidation furnace filled with H_2O vapor and N_2 carrier gas to laterally oxidize the high Al-composition layers in the top p-DBR, the aperture and parasitic reduction oxide layers. Side view scanning electron microscopy (SEM) images of the oxide layers are shown in Fig. 1(b). The p-type Ti/Pt/Au and n-type Ni/AuGe/Ni/Au metal contact was evaporated and annealed, respectively. The device fabrication is finished with benzocyclobutene (BCB) planarization, via-hole etching, and Ti/Au metal interconnect evaporation. Schematic cross-section of the VCSEL structure is shown in Fig.1 (a) and the top-view of VCSEL with ground-signal (GS) Ti/Au probe pads is shown in Fig. 1(c).

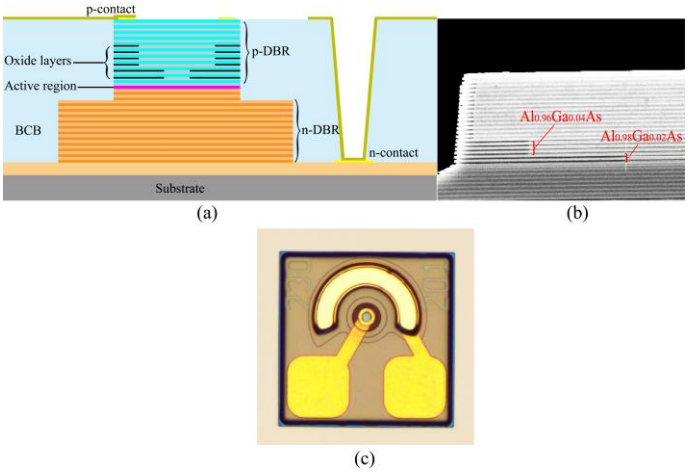

Fig. 1. (a)Schematic cross-section of the VCSEL structure. (b) SEM image of the cross section of the device, the dark lines are the oxidized high Al-composition layers in the p-DBR stack. (c) Top-view of fabricated VCSEL with ground-signal (GS) probe pads.

3. STATIC CHARACTERISTICS

The measured light-current-voltage (L-I-V) characteristics of the VCSELs with oxide-aperture diameters of ~5 μm at different temperature are shown in Figure 2. The threshold current increases from I_{th}= 0.53 mA at 25 ℃ to 0.76 mA at 45 ℃, to 1.05 mA at 65 ℃, and finally to 1.48 mA at 85 ℃. At higher temperatures, the threshold current increases due

to the increased optical absorption, reduced internal efficiency, and an increase of the gain-wavelength detuning (lower gain), and is close to twice the 25℃ value at 85 ℃.

Fig. 3 shows the lasing spectra of the device under the bias of I=1.5 mA (25℃) and I=4.5 mA (85℃). The bias current is about $3I_{th}$. A redshift of 5.38 nm was observed when the bias and temperature condition change.

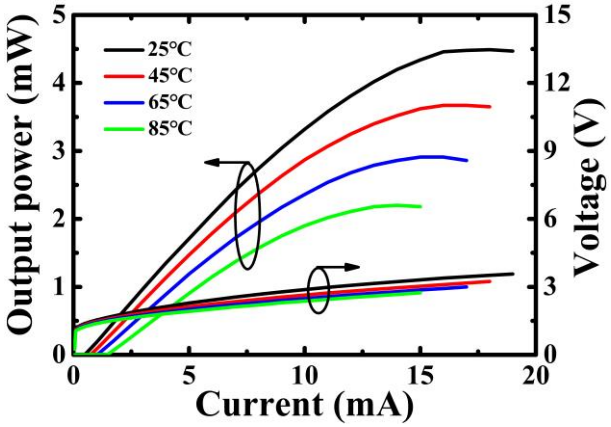

Fig. 2. L-I-V characteristics of the 1030 nm oxide-confined VCSEL from 25℃ to 85℃.

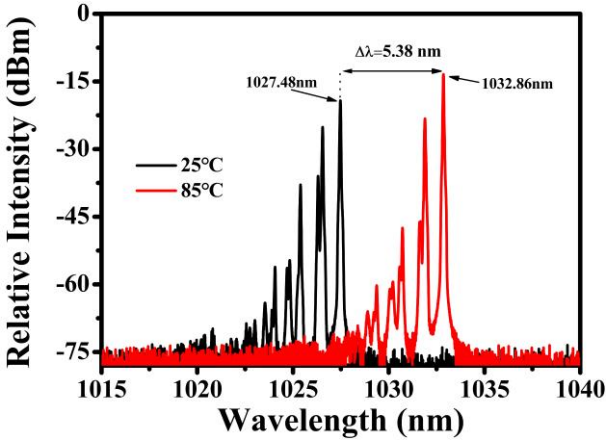

Fig. 3. The optical spectrum of the VCSEL at two biasing and temperature conditions: the black curve represents room temperature measurement at I=1.5mA ($I/I_{th}\approx3$) and the red curve represents 85℃ measurement at I=4.5 mA ($I/I_{th}\approx3$).

4. SMALL-SIGNAL MODULATION

The small-signal modulation response (S21) can be modelled as a second order damped system described by a resonance frequency f_r and a damping rate γ [26]. Accounting for both the intrinsic response of the laser and the extrinsic, parasitic response, giving the full three-pole transfer function

$$H(f) = A \cdot \frac{1}{1 + j(f / f_p)} \cdot \frac{f_r^2}{f_r^2 - f^2 + \gamma \cdot f / 2\pi}, \quad (1)$$

where A is an amplitude factor, f is the modulation frequency, f_p is the parasitic cut-off frequency. The parasitic transfer function may also be determined by S_{11} measurements, which also allow fitting values of the parasitic elements to an equivalent circuit model [27].

The resonance frequency increases linearly with the square root of bias current above threshold according to

$$f_r = D \cdot \sqrt{I - I_{th}} \,. \tag{2}$$

VCSELs with a large D-factor and low threshold current reach high resonance frequencies at low bias currents, which enables energy-efficient high-speed modulation. A large D-factor is also important in order to reach a high maximal VCSEL bandwidth, equivalent to reaching a large resonance frequency before current induced self-heating and thermal saturation deteriorates performance.

The damping is increasing linearly with the square of the resonance frequency and determines an intrinsic upper limit to the modulation bandwidth. The rate at which damping increases is quantified by the K-factor

$$\gamma = K \cdot f_r^2 + \gamma_0 \,, \tag{3}$$

where the offset γ_0 is approximately equal to the inverse differential carrier lifetime [26].

The small signal modulation response was measured using a 67 GHz vector network analyzer (Keysight) connected to the VCSEL under test through a high-speed bias-T and a high-speed RF probe (Picoprobe). The VCSELs were probed directly on wafer and the light was coupled into an angled multimode fiber and then was fed to a 30 GHz photodetector (Thorlabs) via a variable optical attenuator (VOA) to avoid saturation of the detector. The measured data was corrected for the limited frequency response of the probe and detector.

Fig. 4 (a) and (b) show the small signal modulation response (S_{21}) at 25 ℃ and 85 ℃, respectively, and plotted together with fits to a three-pole transfer function (1). The low frequency roll-off which is most pronounced at low bias in Fig. 4 (a) and (b) is attributed to excessive damping from spatial hole burning [28]. The 5 μm aperture VCSEL reaches a maximum bandwidth of 25.1 GHz and 20.6 GHz at 12 mA under 25 ℃ and 85 ℃, respectively.

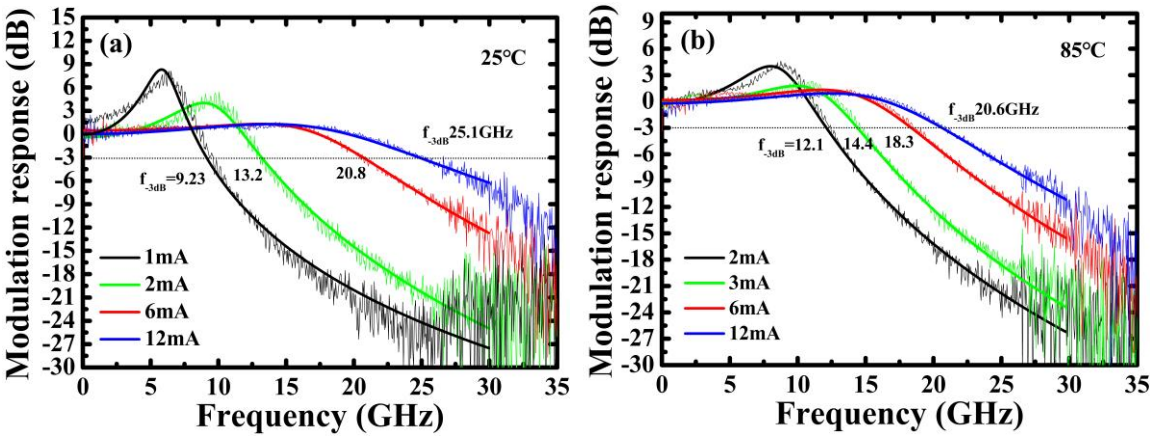

Fig. 4. Small signal modulation response for VCSEL (a) 25°C and (b) 85°C at indicated bias currents.

A three-pole transfer function (1) was fitted to the measured data to extract the resonance frequency and the damping rate. By plotting of resonance frequency (f_r) against $\sqrt{I - I_{th}}$, the D-factor of the VCSEL can be extracted. Fig. 5 shows the resonance frequency (f_r) plotted against the square root of bias current (I) above threshold (I_{th}) under different temperature conditions. The extracted D-factor is 7.8 GHz/mA$^{1/2}$ and the resonance frequency saturates at a maximum value of~22 GHz at 25 ℃. Increasing the temperature to 85 ℃ only results in a minor reduction of the D-factor to 7.2 GHz/mA$^{1/2}$, but since thermal saturation sets in earlier at this temperature, the maximum resonance frequency is reduced more noticeably to~19 GHz. The D-factor is relatively temperature stable, dropping only 14% from 25 to 85 ℃. K-factors were extracted from linear fits of (3) as seen in Fig. 6, and were found to be relatively temperature insensitive at 0.14–0.17 ns from 25 to 85 ℃.

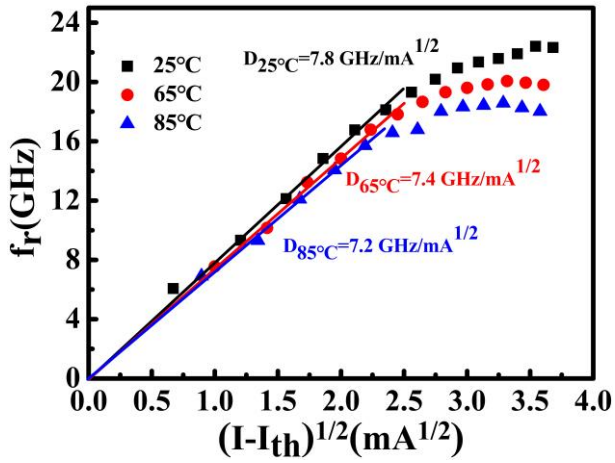

Fig. 5. Fitted resonance frequency, $f_{r,}$ vs. $\sqrt{I-I_{th}}$ plots at 25°C, 65°C, and 85°C. The fitted slope of the data points in the linear region corresponds to the D-factor.

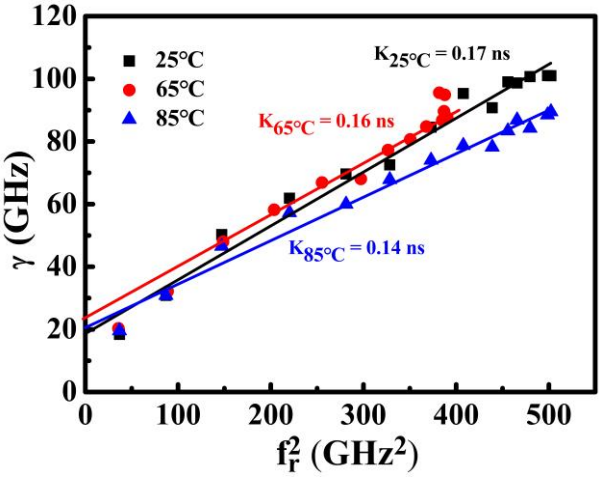

Fig. 6. Fitted damping rate,γ, vs. fitted resonance frequency squared, f_r^2, at 25°C, 65°C, and 85°C.

5. LARGE-SIGNAL MODULATION

To validate the device's data-transmitting capability, we perform the eye diagram and bit-error-rate (BER) measurement. The transmission interconnect setup consists of a SHF Bit Pattern Generator (BPG) that provides the modulation bit sequence, the same light collimation module used for DC and RF measurements, a 2 m optical fiber that collects the coupled light from the light collimation module (referred to as back-to-back (BTB) configuration), and a Thorlabs 30 GHz photoreceiver that converts the collected optical signal back into electrical signal. The test bit sequence used is a non-return-to-zero (NRZ) 2^7-1 by the SHF BPG. The converted electrical signal from the photoreceiver is sent to the SHF Error Analyzer for BER testing. A Tektronix Oscilloscope with a 59 GHz bandwidth sampling module is used to capture the eye diagrams. At I = 10 mA, the VCSEL is able to show an open - "eye" at 40 Gb/s, as shown in the inset of Fig. 7. Fig. 7 shows the measured BER as a function of detected optical power at 40 Gb/s in the BTB configuration, and the device is able to demonstrate error-free (BER < 10^{-12}) transmission at received optical power greater than -2.5dBm at 25℃.

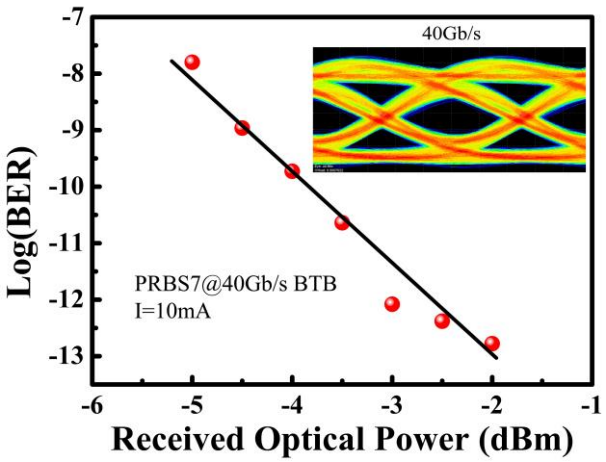

Fig. 7. The 40 Gb/s BER measurement results of the VCSEL biased at 10 mA and tested with PRBS7 bit sequence; the inset is the corresponding eye diagram.

6. CONCLUSION

In conclusion, we have demonstrated a high-speed 1030nm VCSELs with a short optical cavity and multiple oxide apertures. The use of a short λ/2 cavity improves the longitudinal confinement factor and the dynamic properties. To reduce capacitance, we use multiple oxide apertures with two primary apertures for transverse optical and current confinement and four secondary oxide apertures are for parasitic capacitance reduction after oxidation. The 1030 nm VCSEL with ~5 μm aperture was demonstrated a bandwidth of 25.1 GHz at 25 ℃, and can be modulated for error-free data transmission at rates up to 40 Gb/s. Our device is promising to be used as high-speed transmitters in the next generation data centers.

ACKNOWLEDGEMENT

This work was supported by the National key research and development program of China (grant 2018YFB2201000, 2021YFB2801000), the K.C.Wong talent program of Chinese Academy of Sciences (grant GJTD-2020-10), and the Open Fund of State Key Laboratory of High Power Semiconductor Lasers (2022-CCLG-ZDSYS-005).

REFERENCES

[1] J. A. Tatum et al., “VCSEL-based interconnects for current and future data centers,” IEEE J. Lightwave Technol. 33(4), 727-732 (2015).
[2] D. Mahgerefteh et al., “Techno-economic comparison of silicon photonics and multimode VCSELs,” IEEE J. Lightwave Technol. 34(2), 233-242 (2016).
[3] A. Tatarczak et al., “Reach Extension and Capacity Enhancement of VCSEL-Based Transmission Over Single-Lane MMF Links”, IEEE J. Lightwave Technol. 35(4), 565-571 (2017).
[4] M.J. Li, “MMF for high data rate and short length applications,” Proc. Opt. Fiber Commun., 1-3 (2014).
[5] Y. Sun, “Recent advances for high speed short reach optical interconnects for datacom links,” Proc. IEEE CPMT Symp., 63-65 (2017).
[6] M.J. Li, “Novel optical fibers for data center applications,” Proc. SPIE 9772, 977205-1-7 (2016).
[7] S. R. Bickham et al., “Low Cutoff G.657-Compatible Fiber for Data Center Interconnects Operating in the 1064 and 1310 nm Windows,” Proc. SPIE 11286, 112860C-1 (2020)
[8] C. Z. Tong, D. W. Xu, S. F. Yoon, Y. Ding, and W. J. Fan, “Temperature Characteristics of 1.3-μm p-Doped InAs–GaAs Quantum-Dot Vertical-Cavity Surface-Emitting Lasers,” IEEE Journal of Selected Topics in Quantum Electronics. 15(3), 743-748 (2009).

[9] S. Spiga, M. Müller, and M. C. Amann, “Energy-efficient high-speed InP-based 1.3 μm short-cavity VCSELs,” IEEE ICTON, (2013).
[10] A. Malacarne et al., “Optical Transmitter Based on a 1.3-μm VCSEL and a SiGe Driver Circuit for Short-Reach Applications and Beyond,” IEEE J. Lightwave Technol. 36(9), 1527-1536 (2018).
[11] H. Hatakeyama et al,, “Highly reliable high-speed 1.1 μm range VCSELs with InGaAs/GaAsP MQW,” IEEE J. Quantum Electron. 46(6), 890-87 (2010).
[12] J. Guenter, B. Hawkins, R. Hawthorne, and G. Landry, “Reliability of VCSELs for >25 Gb/s,” in Proc. Opt. Fiber Commun., 1–3 (2014).
[13] N. Suzuki, H. Hatakeyama, K. Fukatsu, T. Anan, K. Yashiki, and M. Tsuji, “25 Gbit/s operation of InGaAs-based VCSELs,” Electron. Lett., vol(17), 975–976 (2006).
[14] Y. Zheng, C.H. Lin, A.V. Barve, and L.A. Coldren, “p-type δ-doping of highly strained VCSELs for 25 Gbps operation,” in: Proc. IEEE Photonics Conference, Burlingame, 131-132 (2012).
[15] T. Suzuki, M. Funabashi, H. Shimizu, K. Nagashima, S. Kamiya, and A. Kasukawa, “1060 nm 28 Gbps VCSEL development at Furukawa,” Proc. SPIE 9001, 20-28 (2014).
[16] T. Kise, T. Suzuki, M. Funabashi, K. Nagashima, and H. Nasu, "Development of 1060nm 25-Gb/s VCSEL and Demonstration of 300m and 500m System Reach using MMFs and Link optimized for 1060nm." Optical Fiber Communication Conference. Opt. Communication, paper Th4G-3 (2015).
[17] J. B. Heroux et al., "Energy-efficient 1060-nm optical link operating up to 28 Gb/s." Journal of Lightwave Technology, vol(4), 733-740 (2015).
[18] K. Nagashima, T. Kise, Y. Ishikawa, and H. Nasu, “A Record 1-km MMF NRZ 25.78-Gb/s Error-Free Link Using a 1060-nm DIC VCSEL,” IEEE Photon. Technol. Lett. 28(4), 418–420 (2016).
[19] E. Simpanen et al., “1060 nm VCSEL for up to 40 Gbit/s Data Transmission,” IEEE International Semiconductor Laser Conference, (2016).
[20] A. Larssona et al., “1060 nm VCSELs for long-reach optical interconnects,” Optical Fiber Technology. 44, 36-42 (2018).
[21] E. Simpanen et al., “1060 nm Single-Mode VCSEL and Single-Mode Fiber Links for Long-Reach Optical Interconnects,” J. Lightw. Technol. 37(13), 2963-2969 (2019).
[22] P. Westbergh et al., “High-speed oxide-confined 850 nm VCSELs operating at 40 Gb/s up to 85°C,” IEEE Photon. Techn. Lett. 25(8), 768–771 (2013).
[23] E. Haglund et al., “30 GHz bandwidth 850 nm VCSEL with sub100 fJ/bit energy dissipation at 25–50Gbit/s,” Electron. Lett. 51(14), 1096–1098 (2015).
[24] E. Haglund, P. Westbergh, J.S. Gustavsson, E.P. Haglund, and A. Larsson, “High-speed VCSELs with strong confinement of optical fields and carriers,” IEEE J. Lightwave Technol. 34(2), 269–277 (2016).
[25] N. Haghighi, G. Larisch, R. Rosales, M. Zorn, and J. A. Lott, “35 GHz bandwidth with directly current modulated 980 nm oxide aperture single cavity VCSELs,” IEEE International Semiconductor Laser Conference, 245-246 (2018).
[26] L. A. Coldren, and S. W. Corzine, “Diode Lasers and Photonic Integrated Circuits,” Wiley, New York, 185 (2014).
[27] Y. Ou, J. S. Gustavsson, P. Westbergh, A. Haglund, A. Larsson, and A. Joel, “Impedance characteristics and parasitic speed limitations of high speed 850-nm VCSELs,” IEEE Photon. Technol. Lett. 21(24), 1840–1842 (2009).
[28] Y. Liu, W. C. Ng, B. Klein, and K. Hess, “Effects of the spatial nonuniformity of optical transverse modes on the modulation response of vertical-cavity-surface-emitting lasers,” IEEE J. Quantum Electron. 39(1), 99–108 (2003).